Structural Engineering and Mechanics, Vol. 35, No. 6 (2010) 699-715 699
DOI: http://dx.doi.org/10.12989/sem.2010.35.6.699

Plastification procedure of laterally-loaded steel bars under a rising temperature

*Zhan-fei Huang[1], Kang-hai Tan[2a] and George L. England[3b]

[1]*AECOM Singapore Pte Ltd., BLK. 289G, Bukit Batok St. 25, #07-108, Singapore 656289*
[2]*School of Civil & Environmental Engineering, Nanyang Technological University, Singapore 639798*
[3]*Department of Civil Engineering, Imperial College, Imperial College Road, London SW7 2BU, United Kingdom*

(Received September 10, 2008, Accepted March 9, 2010)

Abstract. This paper investigates the structural responses of axially restrained steel beams under fire conditions by a nonlinear finite element method. The axial restraint is represented by a linear elastic spring. Different parameters which include beam slenderness ratio, external load level and axial restraint ratio are investigated. The process of forming a mid-span plastic hinge at the mid-span under a rising temperature is studied. In line with forming a fully plastic hinge at mid-span, the response of a restrained beam under rising temperature can be divided into three stages, viz. no plastic hinge, hinge forming and rotating, and catenary action stage. During catenary action stage, the axial restraint pulls the heated beam and prevents it from failing. This study introduces definitions of beam limiting temperature $T_{\lim}$, catenary temperature T_{ctn} and warning time t_{wn}. Influences of slenderness ratio, load level and axial restraint ratio on $T_{\lim}$, T_{ctn} and t_{wn} are examined.

Keywords: steel; fire; numerical analysis; axial restraint; limiting temperature; catenary action.

1. Introduction

This paper focuses on the structural behaviour of axially-restrained steel beams under elevated temperature. Unlike under cool environment, a steel beam within a compartment fire received noticeable axial restraint (Fig. 1) from its adjoining cool structure. There are marked differences between the behaviour of a beam subjected to fire attack and the behaviour of the same beam under normal service condition. The response of a heated beam is affected by various factors, such as external load level, boundary restraints, beam slenderness ratio, thermal gradient within the beam, creep, and rate of heating etc. Certainly, a heated beam will receive rotational restraint at two ends contributed by its adjoining beam-to-column connections, and there are strong interactions between the axial and rotational restraints at beam ends. Nonetheless, only axial restraint will be investigated in this study. The influences of rotational restraint on the axial restraint will not be examined either.

*Corresponding author, Former Research Fellow of Nanyang Technological University, E-mail: czf-huang@ntu.edu.sg, Zhanfei.huang@aecom.com
[a]Associate Professor
[b]Emeritus Professor

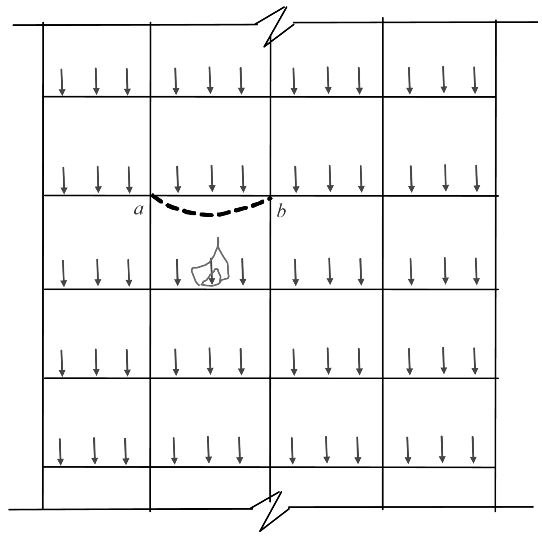

Fig. 1 A compartment fire within a multi-storey steel frame

To date, axial restraint effect on a steel column has been examined both numerically and experimentally (for example, Rodrigues *et al*. 2000, Huang *et al*. 2006, Tan *et al*. 2007). This is due to the fact that columns play a more important role than beams in terms of structural safety. In contrast, there are limited published works on the influence of axial restraint on the beam response in fire. The following briefs a recent research works on this aspect.

In the experimental aspect, Liu *et al*. (2002) reported a series of fire tests to study axial restraint effect on unprotected steel beams. Three axial restraint ratios were investigated. Both flush end-plate beam-to-column connection and web-cleat connection were examined. Three different load levels were applied onto the heated beams. The development of internal axial force in members was obtained. It is also observed that catenary action prevented the beams from failing mechanically. Local buckling occurred on nearly all beams with end-plate connections while it seldom occurred in beams with web-cleat connection. However, local buckling did not lead to immediate or premature failure in those beams with end-plate connection. Catenary action, which was mobilized at large deflection, was observed in beams with high axial restraint and subjected to low load levels. In 2008, six steel sub-frames were tested under natural fire in Portugal (Santiago *et al*. 2008). Influences of beam-to-column connections on the behaviour of sub-frames were examined.

In the analytical aspect, Yin and Wang (2004) proposed a simple analytical model to compute the catenary forces in steel beams at elevated temperature. Both axial and flexural restraints at the beam ends were considered. The deflection of a beam was approximated as a polynominal curve for pinned-pinned (no rotational restraint) and fixed-fixed (full rotational restraint) beams under uniformly distributed load. For a beam with limited rotational restraint, linear interpolation was adopted as a function of rotational restraint stiffness. Validation of the proposed method showed that normally the predicted catenary force was greater than the associated numerical results.

In Australia, Wong (2005) proposed a formula to calculate limiting temperature of axially-restrained steel beams. He also presented a simple technique to quantify the axial restraint exerted onto a heated beam from its neighbouring members. The axial force induced by thermal expansion was incorporated through axial-bending interaction of a critical cross section. It was assumed that the shear force present at a section is negligible compared to the axial force and bending moment values. The catenary action of beams was also considered. Nevertheless, beneficial effects from rotational restraints at both ends were not considered.

Bradford (2006) derived a generic modelling of axially and flexurally-restrained steel beams at elevated temperature. The analysis was elastic and therefore yielding and catenary action were ignored. Based on theorem of virtual work, governing differential equations were derived and solved for specific cases of restraint stiffness.

To make use of catenary action in the fire resistant design of steel beams that may substantially decrease fire protections to the beams, the plastification process of an axially-restrained steel beam at elevated temperature should be understood fundamentally. This becomes the objective of this study.

This paper presents numerical simulation for examining the structural response of restrained square steel beams at elevated temperatures. The investigated parameters include the beam slenderness ratio λ, load utilization factor μ and axial restraint ratio β_l. At the end of the paper, beam limiting temperatures $T_{\lim}$ and catenary temperature T_{ctn} of all cases are plotted for reference. Nevertheless, it should be pointed out that similar to any other studies, numerical observations from this study which are based on assumptions (see Sec. 2 & 3) should be justified when they are applied to other conditions æ under those conditions, these observations are more instructive than conclusive.

2. Isolated axially-restrained beam model and scope of analyses

To study the axial restraint effect on a heated beam, an isolated beam model is proposed as shown in Fig. 2, in which a linear spring is used to simulate the axial restraint exerted on the beam. For consistency, in all the following case studies a square steel section of 100×100 mm^2 is adopted. The choice of square cross section is incidental; the general observations are instructive to other types of cross section. Nevertheless, due to stark difference of shape factors among sections (Horne and Morris 1981), plastification process of a member with a non-square section (say, I-section) tends to be somehow different.

Three series of beams, with respective slenderness ratio λ of 40, 80 and 120, will be examined. The slenderness ratios considered nearly cover the practical design range. Each series contains 6 groups of beams with different axial restraint ratio β_l varying from 0, 0.01, 0.1, 0.5, 1.0 and ∞ (infinity). The range of β_l represents a whole gamut of restraints while the practical range of β_l is unavailable. Here, β_l is defined as the ratio of linear spring stiffness to beam axial stiffness. That is,

$$\beta_l = \frac{k_l}{E_0^{20} A_b / l_b} \tag{1}$$

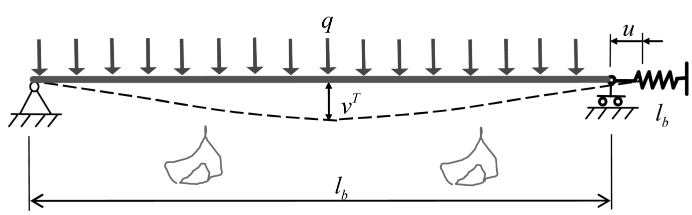

Fig. 2 Isolated axially-restrained beam model

in which the denominator $E_0^{20}A_b/l_b$ represents the beam axial stiffness at 20°C, E_0^{20} is elastic modulus of steel at ambient temperature, A_b is the cross sectional area and l_b is beam span.

Within each group, beams of the same β_l are subjected to 7 different external load levels (termed as R) that increases from zero to 0.7 at a constant increment of 0.1. In terms of loading pattern, only uniformly distributed lateral load (hereafter, UDL) is considered. The load level R is defined as the ratio of mid-span bending moment for a pinned-rollered beam to its cross-sectional plastic moment capacity M_p^{20} in the absence of axial force. That is

$$R = \frac{ql_b^2}{8M_p^{20}} = \frac{ql_b^2}{8f_y^{20}W_p} \tag{2}$$

where q is UDL value, W_p plastic modulus of a section. For a square section, $W_p = a^3/4$, where a is the sectional dimension.

3. Assumptions

In the numerical simulation, some assumptions have been made as follows:

1. The beams are assumed to be perfect, i.e., the initial out-of straightness, and the residual stresses within a member are not taken into account.

2. The beams are restrained transversely (out-of-plane), thus neither local nor lateral-torsional buckling is considered. This assumption is reasonable as most beams are restrained by the slabs on top. Besides, local buckling of the web and/or bottom flange due to compression in fire, in a fire engineering approach, is not considered as a failure mode since further increase of temperature after it takes place will cause the beam to develop catenary action to support transverse loadings. Hence, influence of local buckling is desirable rather than unfavourable.

3. Rotational restraints at beam ends are not considered. The restraint tends to generate compression at the bottom flange of an I-beam and mobilize local buckling of the flange. This phenomenon is popular in beams with end-plate connections (Liu *et al*. 2002).

4. Linear springs are assumed to be elastic throughout a heating, that is, its stiffness k_l remains unchanged. This is reasonable in practice as under most fire conditions, the adjoining structure is hardly affected and the horizontal movement of a heated beam is normally very small. Hence, the axial spring responds elastically.

5. Throughout heating, there is no failure at the beam-to-column joint. It should be pointed out that during realistic fire attack or experiment, failure of beam-to-column joints has indeed been observed (Wald *et al*. 2006). Extensive study of different beam-to-column connections behaviour under fire attack is being carried out throughout the world, and a latest review can be found from Al-Jabri *et al*'s work (Al-Jabri *et al*. 2008). At the current stage, a 3-D FE model (Liu 1996) or component-based model provides two most popular means for a reliable examination of connection response in fire. The former probably requires advanced FE knowledge (Sarraj *et al*. 2007) and demands huge preparation works and analysis efforts as well. The latter is still being developed and is rarely used. Due to the complexity nature of beam-to-column connection response in a fire (Al-Jabri *et al*. 2008, Ramli-Sulong *et al*. 2007), connection flexural stiffness is not considered nor is joint failure accounted for in this study. This is to maintain the simplicity of this study and to focus on behaviour of a heated beam rather than its framing connection.

6. Temperature across a beam section as well as along its length is uniformly distributed. In steel

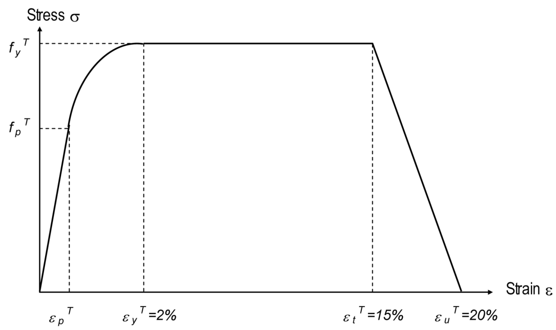

(a) σ-ε relationship

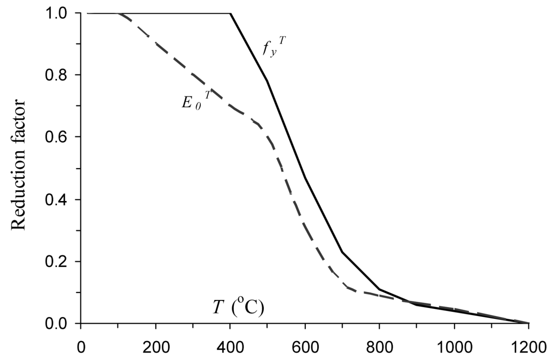

(b) Reduction factor

Fig. 3 EC3 steel material model at elevated temperature (CEN 2000)

structures most beams are composite ones with top flanges encased in or supporting an RC slab. As such, thermal gradient along the beam depth will be presented under a fire attack. Effects of thermal gradient on the behaviour of steel beam have been studied (Burgess *et al*. 1991, Wang *et al* 1995, Tan and Huang 2005). Acknowledged the above fact, effect of the thermal gradient is not presented in this paper.

7. Steel temperature rises monotonically until the beam fails; that is, no cooling effect is accounted for. The latest progresses on the study of steel beam response during cooling stage can be found in Wang *et al*. (2008) and Li and Guo (2008, 2009). Cooling effect, due to its nature of complexity, deserves a separate investigation and thus is excluded from this study.

8. EC3 steel model (CEN 2000) is employed in this study. EC3 model adopts bilinear-elliptical stress-strain relationship at elevated temperature (Fig. 3(a)). No strain-hardening is considered. The reduction factors of yield strength f_y^T and elastic modulus E_0^T at elevated temperature are shown in Fig. 3(b).

In FE analysis, each beam is divided into 10 elements of equal length. A self-developed FE program titled FEMFAN is used in this study (Tan *et al*. 2002). It is capable of elasto-plastic and creep analysis of steel plane frames at elevated temperatures. Both material and geometrical nonlinearities are considered. It employs layered co-rotational beam element which is able to capture accurately the cross-sectional thermal gradient and plastification process.

4. Failure criterion

Fig. 4 shows that at the instant when a plastic hinge forms at the beam mid-span, there are 5 types of cross-sectional stress distribution along the beam length. Due to symmetry in geometry and loading, only half of the beam is considered.

Fig. 4 shows that within any cross section between point '*O*' and '*A*', neither extreme fibres in compression zone nor those in the tension stress zone yield. At point '*A*', the top fibre in compression just yields. From point '*A*' to '*C*', with increasing applied moment M_c^T (subscript *c* denotes presence of compression force) and subjected to constant axial force, yielding gradually spreads from the compression to tension zone. Finally and right at point '*C*', the whole section becomes fully plastic.

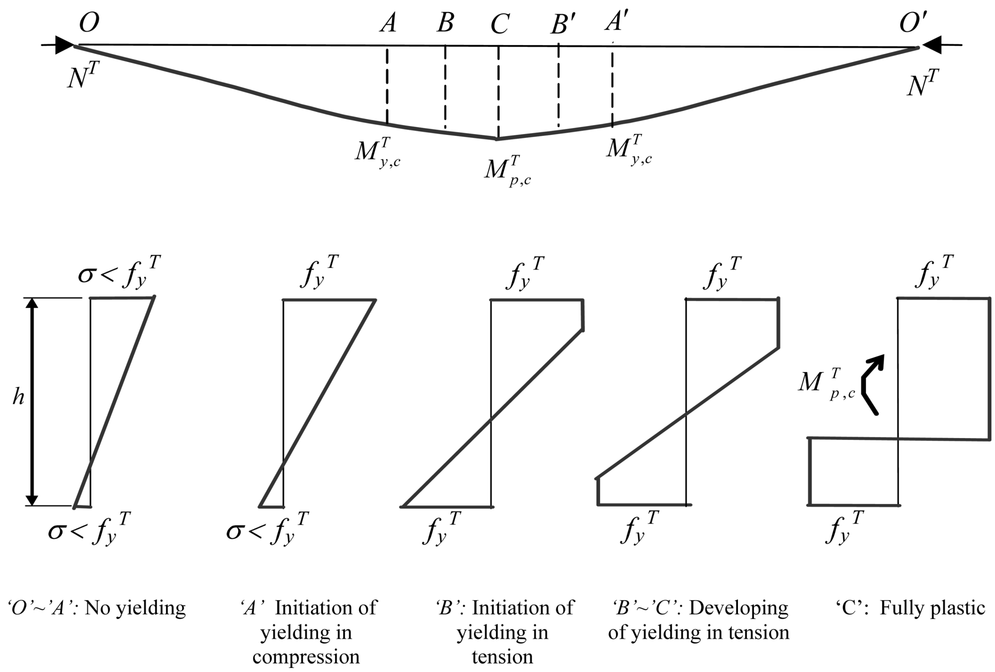

Fig. 4 Cross-sectional stress distributions along a beam when mid-span is fully plastified

In the presence of internal axial force N^T, the *reduced plastic moment capacity* $M^T_{p,c}$ for the square section can be expressed as (Horne and Morris 1981)

$$\xi^T = (\rho^T_N)^2 + \rho^T_M = 1 \tag{3}$$

where $\rho^T_N = N^T/N^T_y$, $\rho^T_M = M^T_{p,c}/M^T_p$ and ξ^T denotes the plasticity index taking account of interaction between axial force N^T and bending moment $M^T_{p,c}$.

With a plastic hinge forming at point '*C*', any attempt to increase the moment further will cause the member to rotate at point '*C*'. The beam will survive under the pulling force from the boundary restraint, this is termed as catenary action.

In the numerical analysis, Eq. (3) is adopted as a criterion that indicates the formation of plastic hinge. Due to potential numerical error, this study assumes that as long as ξ^T achieves 0.98, a plastic hinge forms.

5. Collapse process of a general beam

5.1 Overall behaviour of λ = 40 beam with β_l = 0.5

Firstly, a stocky beam of $\lambda = 40$ is chosen for study. This beam receives with $\beta_l = 0.5$ is subjected to a moderate load level of 0.5. The numerical results are shown in Fig. 5, in which Fig. 5(a) shows the development of three indices ρ^T_N, ρ^T_M & ξ^T at the mid-span during the heating, Fig. 5(b) shows the internal axial force N^T and mid-span moment M^T and Fig. 5(c) the mid-span deflection v^T and

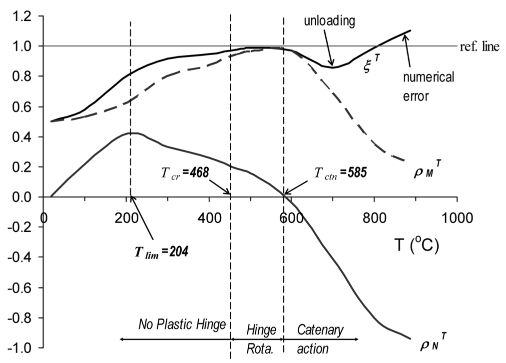

(a) ρ_N^T, ρ_M^T & ξ^T (β_l=0.5)

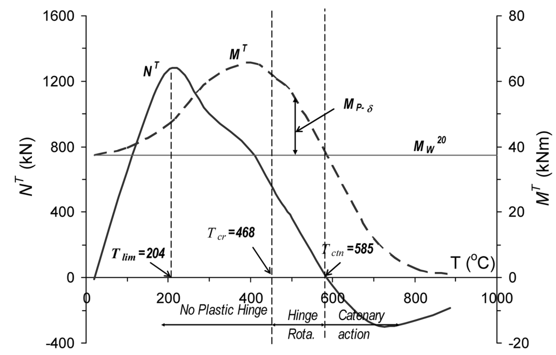

(b) N^T & M^T (β_l=0.5)

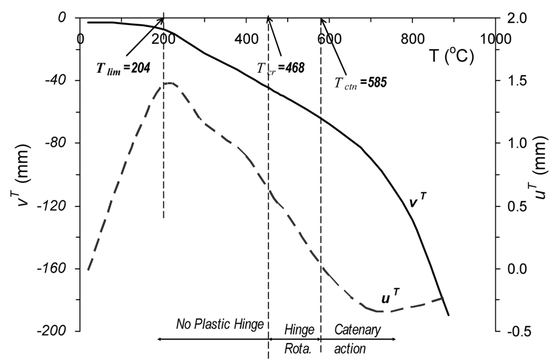

(c) v^T & u^T (β_l=0.5)

Fig. 5 Developments of internal forces and deflection in $\lambda = 40$ beam with $\beta_l = 0.5$ under a rising temperature (load level $R = 0.5$)

right-end expansion u^T.

Generally, the collapse behaviour of the heated beam can be divided into three stages, namely, no plastic hinge stage, hinge formation and rotation stage, and catenary action stage.

Fig. 5(a) shows that during the first stage, axial index ρ_N^T increases nearly linearly to around 204°C, after which ρ_N^T decreases all the way. Beyond 585°C, ρ_N^T changes its sign from compression to tension. At the same time, moment index ρ_M^T increases monotonically from 0.50 to 0.9442 at 468°C, while the plastification index ξ^T progresses from 0.50 to 0.98 signifying formation of a plastic hinge at mid-span. On the other hand, the axial force N^T linearly increases to 1274 kN at 204°C and then decreases to 482 kN at 468°C (Fig. 5(b)). During the first stage, the mid-span moment M^T increases slightly from 37.5 kNm to 47.1 kNm. Theoretically, at a particular temperature M^T comprises two parts as shown below

$$M^T = M_V^T + M_{P-\delta}^T \tag{4}$$

where

$$M_V^T = \frac{q(l_b^T)^2}{8} = \frac{ql_b^2}{8}(1+\alpha\cdot\Delta T)^2 \approx \frac{q(l_b)^2}{8} = M_V^{20} \tag{5}$$

$$M_{P-\delta}^T = N^T \cdot v^T \tag{6}$$

Clearly, M_V^T is induced by UDL while $M_{P-\delta}^T$ is due to $P-\delta$ effect. Fig. 5(c) demonstrates that v^T increases at an accelerating rate during the first stage due to increasing $P-\delta$ effect arising from compressive force N^T. The axial expansion of beam u^T develops in the same manner as N^T (Fig. 5(b)) due to axial restraint.

In this paper, 204°C is defined as the beam *limiting temperature* $T_{\lim}$, at which the internal axial force N^T and longitudinal expansion u^T both attain their respective maximum values. It should be pointed out that for a practical load level R (normally, less than 0.6), all beams under investigation do not form a plastic hinge at mid-span under $T_{\lim}$. As such, limiting temperature $T_{\lim}$ has not been given adequate attention in previous numerical studies. Under an actual fire, a heated steel beam will push away its adjoining columns to the greatest distance at $T_{\lim}$. In the other words, the columns may experience the greatest $P-\Delta$ effect at that moment. In addition, numerical analyses has shown that a heated beam may buckle like a column due to high internal compression force, this tendency being greater for non-symmetric sections such as I-section, channel and Z-sections, which are pone to distorsional or local buckling (Lee 2004).

On the other hand, the temperature associated with the formation of a plastic hinge forms is defined as beam *critical temperature* T_{cr}. T_{cr} is characterised by index ξ^T attains unity. Nevertheless, this definition does not mean the beam fails as the axial restraint will prevent the beam from collapsing through catenary action. Introducing such a definition is merely to establish a convenient basis for numerical study and comparison. Based on the assumption of elastic spring (Fig. 2), the heated beam can only fail due to material fracture under very high temperature.

When temperature rises beyond T_{cr}, the beam enters into its second stage. During this stage, index ξ^T remains at unity while index ρ_N^T decreases steadily to zero and ρ_M^T slightly increases up to unity. Fig. 5(b) shows that during the second stage at the mid-span both N^T and M^T keep on decreasing while the beam experiences plastic hinge rotation. Due to a decreasing N^T, the $P-\delta$ effect is diminishing. In terms of deformation, the beam continues the behaviour during the later period of

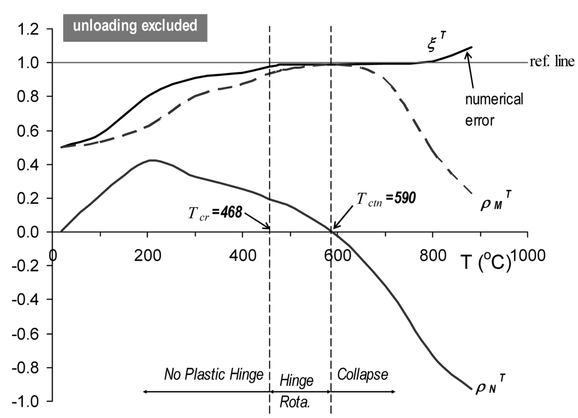

(a) ρ_N^T, ρ_M^T & ξ^T (β_l=0.5)

Fig. 6 Developments of plastification indices for $\lambda = 40$ beam with $\beta_l = 0.5$ under a rising temperature (load level $R = 0.5$, unloading excluded)

Stage-1 - that is, although the beam continues to deflect, the beam end also continues to contract at a steady rate (see u^T and v^T in Fig. 5(c)). This leads to a net increase in M^T, and consequently in ratio ρ_M^T. Fig. 6 shows that axial force N^T, ratio ρ_N^T and horizontal displacement u^T reduce steadily while ξ^T is maintained at unity during this stage.

At the end of stage-2, axial force N^T finally reduces to zero. This signifies the beginning of stage-3 when the beam experiences catenary action. In this study, the temperature at which N^T decreases to 0 is defined as *catenary temperature* T_{ctn}. Obviously, beams with different axial restraint ratios but subjected to the same load level R have a typical T_{ctn}.

The mid-span bending moment at T_{ctn} is computed as

$$M_V^{T_{ctn}} = \frac{q(l_b^T)^2}{8} = \frac{ql_b^2}{8}(1+\alpha\cdot\Delta T)^2 \approx \frac{q(l_b)^2}{8} = M_V^{20} \tag{7}$$

and

$$M^{T_{ctn}} = M_p^{T_{ctn}} = f_y^{T_{ctn}} W_p = (\psi_{f_y}^{T_{ctn}} f_y^{20})\cdot W_p \tag{8}$$

in which W_p is section plastic modulus and $\psi_{f_y}^{T_{ctn}}$ is reduction factor for steel yield strength at T_{ctn}.

By equating Eq. (7) and Eq. (8), there is

$$\psi_{f_y}^{T_{ctn}} = \frac{ql_b^2}{8f_y^{20}W_p} = R \tag{9}$$

Eq. (9) implies that T_{ctn} is the temperature at which the reduction factor $\psi_{f_y}^{T_{ctn}}$ is same as load factor R. For current case with $R = 0.5$, the predicted catenary temperature T_{ctn} is 585°C, very close to 590°C at which $\psi_{f_y}^{T_{ctn}} = 0.5$. The negligible difference of 5°C is attributable to stress unloading at the top half of the section, where tension effect from N^T becomes the dominant one compared to compression effect from M^T.

A beam attains its T_{ctn} when either one of the following criteria is met:

• Internal axial force N^T reduces to zero, and so do parameters ρ_N^T and $M_{p-\delta}$;
• Mid-span moment M^T resorts to its initial value M_V^{20} before heating begins;
• Ratio ρ_M^T increases up to 1.0.

When the heated beam experiences catenary action, it enters Stage-3. During this stage, ρ_N^T becomes negative (note: tension force) and its value keeps on reducing. Moment index ρ_M^T also reduces steadily while ξ^T decreases first and then increases above 1.0 beyond 800°C. The decrement of ξ^T below unity is due to stress unloading at the top half part within a cross section nearly mid-span of the beam. This can be confirmed by the following examination. If unloading is not considered, that is, a nonlinear elastic unloading of stress is adopted, the beam shows a slightly different behaviour during Stage-3. Fig. 6 which shows the developments of three indices illustrates that instead of reducing below 1.0, ξ^T remains at unity during Stage-3 before 800°C. Beyond 800°C, ξ^T rises above 1.0. Again, this is due to numerical error in computing very small M^T (Fig. 5(b)).

Fig. 5(b) shows that beyond T_{ctn}, the tensile axial force N^T increases first and then decreases while bending moment M^T decreases to zero until the beam fails. The beam continues to deflect steadily while it begins to contract axially (Fig. 5(c)). During this stage, from the free body diagram the tension force in the beam can be approximated as

$$N^T = \frac{M_V^{20} - M^T}{v^T} \tag{10}$$

where M_V^{20} is mid-span bending moment before heating starts (Eq. (5)). That is, there is beneficial effet from tension action to counteract the initial imposed M_V^{20}.

At the end of heating, M^T approaches zero and thus

$$N^T \approx \frac{M_V^{20}}{v^T} \tag{11}$$

Eq. (11) explains why beyond 700°C with deflection v^T keeps on increasing, N^T decreases accordingly.

5.2 Mid-span plastification process on λ = 40 beam with β_l = 0.5

It is desirable to have a deeper understanding of the response of beam throughout the heating. This section focuses on the plastification process at the mid-span section. Fig. 7(a) plots out the distribution of midspan sectional stress σ^T at point 'C' of the beam, while Fig. 7(b) depicts the associated ratio of σ^T to the yield strength f_y^T. It is shown that at 20°C, the whole section responds elastically. With temperature increasing up to 314°C, the top edge fibre yields under the actions of N^T and M^T, both of which generate compression strains on the fiber. Further increasing the temperature to 440°C, the bottom edge fiber begins to yield also while more top fibres enter plastification phase. At 585°C when catenary action starts, about half area of the whole cross section becomes plastic. Beyond 585°C, the compression zone of the section keeps on shrinking and finally at 774°C, every fibre within the section experiences tensile stress. Eventually at 861°C, the beam fails due to the bottom edge fibre fracture as the associated tensile strain exceeds 0.20, the ultimate strain ε_u^T (CEN 2000).

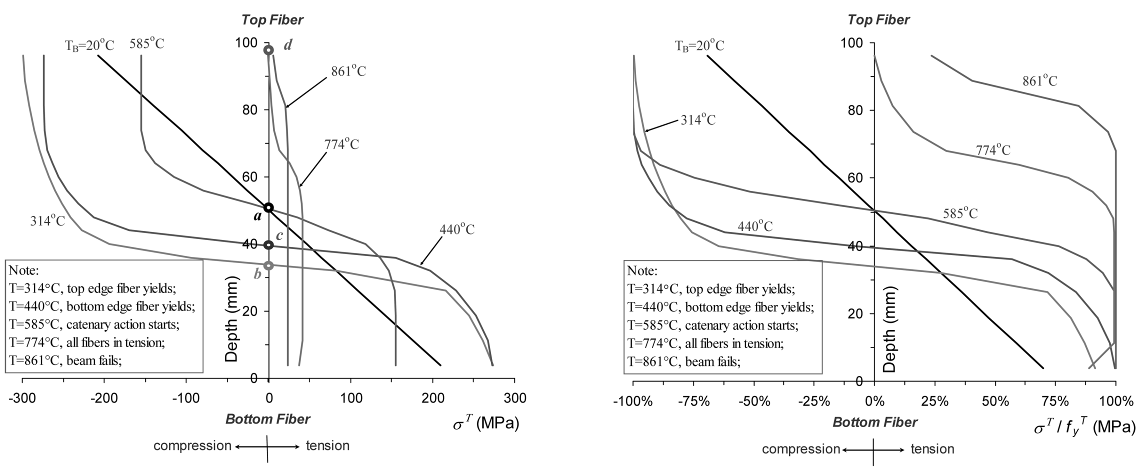

(a) Stress

(b) Stress / yield strength

Fig. 7 Stress distribution within mid-span cross-section in $\lambda = 40$ beam with $\beta_l = 0.5$ under a rising temperature (load level $R = 0.5$)

There are a few noteworthy points in Fig. 7 as listed below:

- From 314°C onwards, the top edge fiber changes from compressive yield strength to tensile stress. Obviously, during this process significant unloading occurs;
- The bottom part of cross section only experiences compressive stress.
- Throughout the heating, Fig. 7(a) shows that the neutral axis (associated with zero stress) moves from the mid-depth point ‘a’ at 20°C down to its lowest position ‘b’ at 314°C, before climbing up to its highest position ‘d’ at 774°C. Beyond 774°C, the neutral axis moves out of the section.

5.3 Axial restraint effect

Entire collapse process of a $\lambda = 40$ beam with limited axial restraint of $\beta_l = 0.5$ has been examined in Sec. 5.1 & 5.2. For the completeness of study, it is useful to conduct FE analyses on the axial restraint effect. Two extreme cases are chosen, viz., a beam with full restraint and the other one without. Load level is remained at 0.5 for both beams. The response of the fully-restrained beam and non-restrained beam is shown in Fig. 8 and Fig. 9, respectively.

Firstly, the fully-restrained beam is taken for study. Fig. 8 shows that this beam responds in a similar manner to the previous beam with $\beta_l = 0.5$ (Fig. 5). They start to experience catenary action

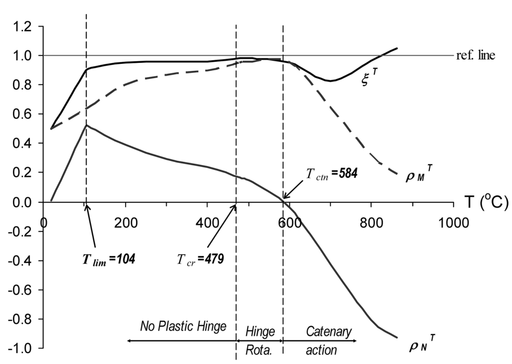

(a) ρ_N^T, ρ_M^T & ξ^T (β_l=∞)

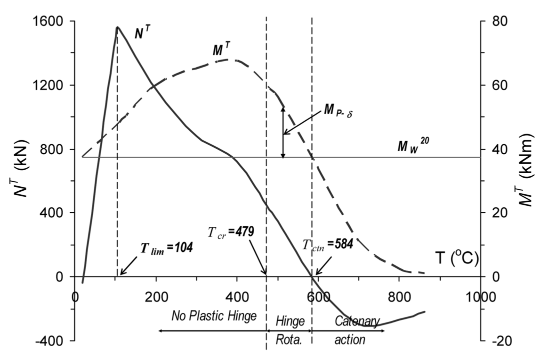

(b) N^T & M^T (β_l=∞)

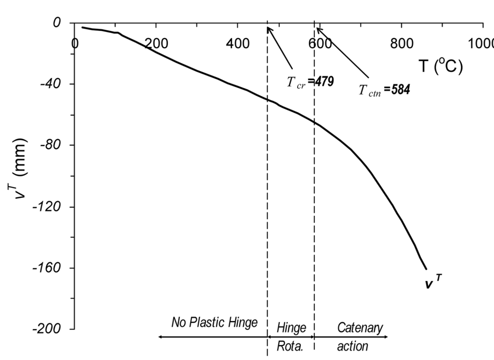

(c) v^T & u^T (β_l=∞)

Fig. 8 Developments of internal forces and deflection in $\lambda = 40$ beam with fully axial restraint under a rising temperature (load level $R = 0.5$)

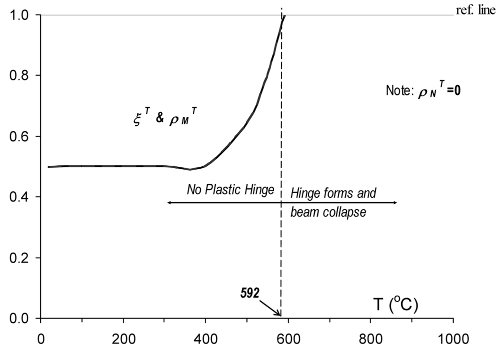

(a) ρ_N^T, ρ_M^T & ξ^T (β_l=0.0)

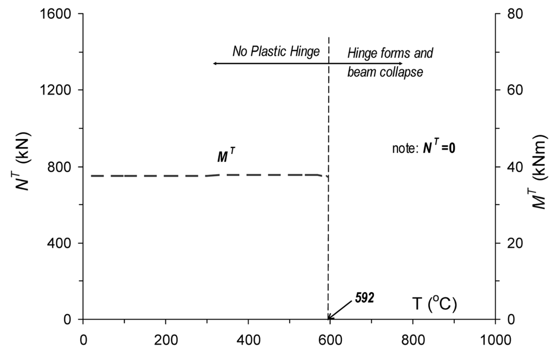

(b) N^T & M^T (β_l=0.0)

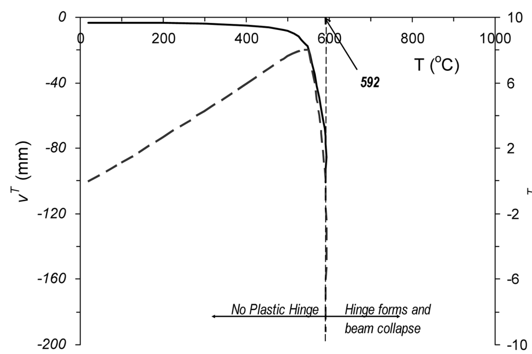

(c) v^T & u^T (β_l=0.0)

Fig. 9 Developments of internal forces and deflection in $\lambda = 40$ beam without axial restraint under a rising temperature (load level $R = 0.5$)

nearly at the same temperature (484°C vs 485°C), which was defined as the catenary temperature T_{ctn}. Nevertheless, although the axial restraint ratio β_l has negligible effect on T_{ctn}, it remarkable reduces the limiting temperature $T_{\lim}$ at which N^T achieves its maximum value in compression. $T_{\lim}$ of the current beam attains 104°C, a significant drop from 204°C attained by the previous beam with $\beta_l = 0.5$ (cf. Fig. 5(a)). Furthermore, this study adopts a concept of *warning time* t_{wn}, which is the time difference between the *catenary time* t_{ctn} and the *limiting time* $t_{\lim}$ associated respectively with T_{ctn} and $T_{\lim}$, respectively. Clearly, by increasing β_l from 0.5 to infinity, t_{wn} is substantially increased since $T_{\lim}$ occurs much earlier (compare Fig. 5(b) and Fig. 8(b)).

In addition, comparison between Fig. 5(b) and Fig. 8(b) illustrates that under the fully restrained condition, the heated beam experiences much more $P-\delta$ effect, represented by an increase in $M_{P-\delta}$. This is directly owing to the greater axial force N^T attained by the fully-restrained beam.

With regard to mid-span deflection v^T, there is little difference between the two beams.

After studying the fully-restrained beam, it is time to examine the beam without restraint. This beam shows a very different behaviour at elevated temperature. Without axial restraint, the beam collapses as soon as a plastic hinge forms at the mid-span (at 592°C). Neither $P-\delta$ effect nor catenary action is experienced. At the end of heating, the mid-span deflection v^T experiences run-away failure (Fig. 9(c)). It should be highlighted that there is no warning time t_{wn} in this beam. That is, this beam will fail in brittle manner which should be avoided in structural fire resistance design.

6. Limiting temperatures

6.1 λ = 40 beams

Limiting temperatures $T_{\lim}$ of 6 groups of axially-restrained beams subjected to different load levels versus parameter ρ_M^{20} are shown in Fig. 10. Here, $\rho_M^{20} = M_{p,c}^T / M_p^{20}$ where M_p^{20} is sectional plastic moment capacity at ambient temperature without presence of axial force. For reference, ψ_{f_y}, the reduction factor for yield strength f_y^T at elevated temperature, is also shown. The ψ_{f_y} curve can also be approximated as catenary temperature T_{ctn} curve for all beams since axial restraint has little effect on T_{ctn} (Sec. 5.1).

Fig. 10 discloses that

- The stiffness the restraint (or the greater the β_l), the lower is the value of $T_{\lim}$.
- The higher the load level R, the lower is the $T_{\lim}$ and the shorter is warning time t_{wn};
- $T_{\lim}$ to a beam with very soft restraint tends to approach T_{ctn} which still slightly greater than $T_{\lim}$. In the other words, a beam with weak axial restraint has less warning time t_{wn} compared to one with strong restraint.

Fig. 10 also plots another series of horizontal curves comprising 7 critical values of R ranging from 0.1 to 0.7. These curves show that:

- For the same R, nearly the same ρ_M^{20} is attained by beams with different restraints;
- The higher the load level R, the greater ρ_M^{20} is achieved at $T_{\lim}$.

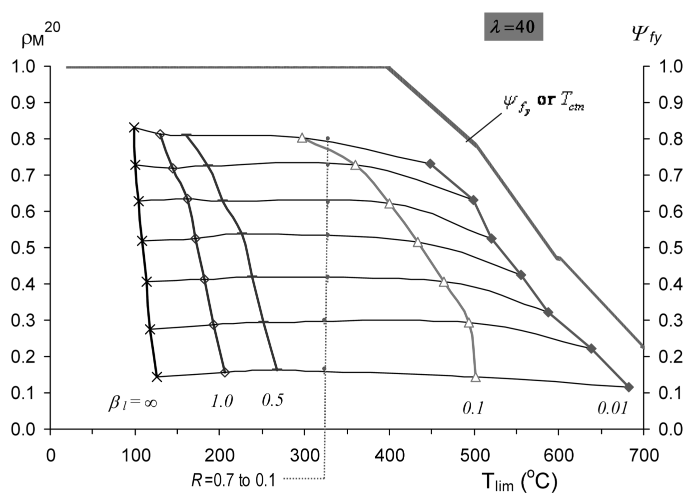

Fig. 10 Limiting and catenary temperatures for $\lambda = 40$ beams

6.2 λ = 80 and λ = 120 beams

Limiting temperatures $T_{\lim}$ of $\lambda = 40$ beams have been predicted in Sec. 6.1. It is equally important to predict $T_{\lim}$ of more slender beams which are also practical in construction. As such, responses of $\lambda = 80$ and 120 beams under elevated temperature are analysed. Similar to $\lambda = 40$ beams, β_l ranges from 0 to infinity and R varies from 0.1 to 0.7. Fig. 11 and Fig. 12 show $T_{\lim}$ and T_{ctn} for $\lambda = 80$ and 120 beams, respectively. Although one has similar observations in Figs. 11 and 12 as in Fig. 10 ($\lambda = 40$ beams), there are some different observations arising from the greater slenderness ratio:

- For the same axial restraint ratio β_l, a slender beam attains lower $T_{\lim}$, especially at high load level. This is due to the more significant $P-\delta$ effect exercised in the slender beam. Therefore,
- Compared to a stocky beam, a slender beam has longer warning time t_{wn};

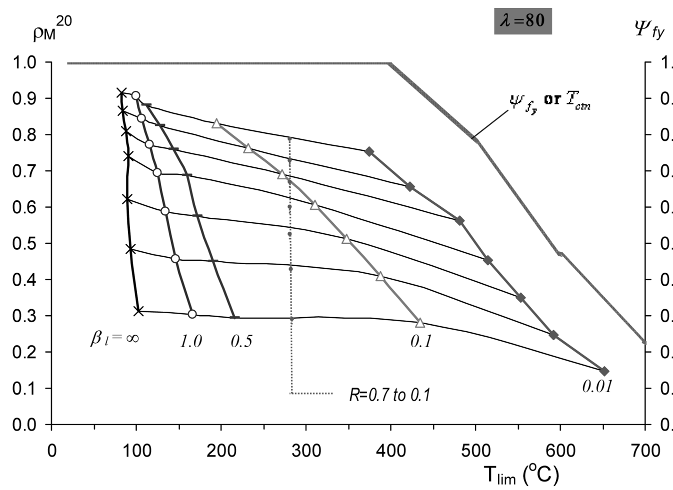

Fig. 11 Limiting and catenary temperatures for $\lambda = 80$ beams

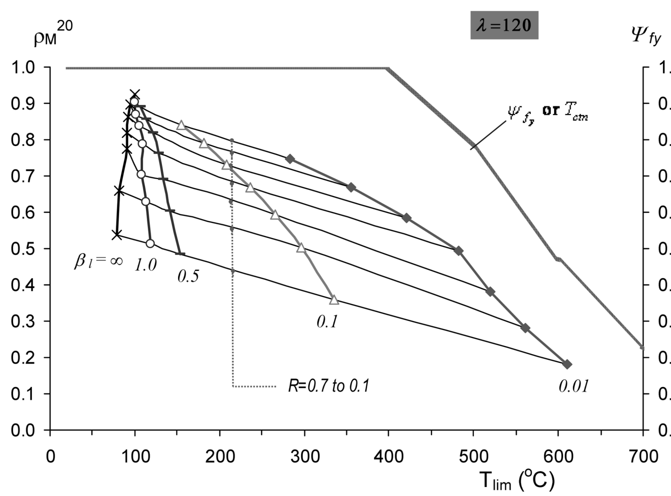

Fig. 12 Limiting and catenary temperatures for $\lambda = 120$ beams

- Under the same load level R, the stiffer the restraint, the greater is ρ_M^{20} due to the more significant $P-\delta$ effect.

7. Conclusions

This paper presents a systematic numerical study on the progressive collapse process of a uniformly heated axially-restrained steel beam under a rising temperature but subject to constant external lateral load. Some important parameters have been examined, viz beam slenderness ratio, external load level and axial restraint ratio.

Forming and developing a plastic hinge at beam mid-span is examined first. It is found that the response of a restraint beam can be divided into three stages: no plastic hinge, hinge forming and rotating, and catenary stages. Catenary stage is signified by the boundary axial restraint starts to pull the heated beam at large deflection. This leads to the restrained beam failing at very high temperature.

This study defines the temperature corresponding to the internal axial compression force reaching its ultimate value as limiting temperature $T_{\lim}$. The temperature when catenary action begins is defined as catenary temperature T_{ctn}. FE simulations show that:

- Increasing axial restraint will reduce $T_{\lim}$, while increasing beam slenderness ratio leads to a lower $T_{\lim}$;
- A beam receiving stronger restraint has a longer warning time t_{wn} (as defined in Sec. 5.3);
- Under the same load level R and axial restraint ratio β_l, a slender beam has longer warning time t_{wn}.

Last but not least, it is worthy to note that in reality behaviour of a steel beam under fire condition is strongly affected by other factor such as uneven heating across and along the beam, complicated response of two connections at beam ends and interactions between the beam and its framing RC slab, etc. Furthermore, since behaviour of a restrained beam during cooling stage can be different to that during heating stage (Li and Guo 2009), it should be highlighted that the findings in this study are applicable to heating stage only.

Acknowledgements

The authors would like to express their appreciation to Nanyang Technological University and Defence Science and Technology Agency (Singapore) which sponsor the research (ECAMS grant no: PTRC-CEE/DSTA/2006.03).

References

Al-Jabri, K.S., Davison, J.B. and Burgess, I.W. (2008), "Performance of beam-to-column joints in fire – A review", *Fire Safety J.*, **43**, 50-62.

Bailey, C.G. (2000), "The influence of the thermal expansion of beams on the structural behaviour of columns in steel-framed structures during a fire", *Eng. Struct.*, **22**, 755-768.

Bradford, M.A. (2006), "Elastic analysis of straight members at elevated temperatures", *Adv. Struct. Eng.*, **9**(5),

611-618.
BSI (1987), British Standard BS476, Part 20: Method for determination of the fire resistance of elements of construction, London, U.K.
Burgess, I.W., Rimawi, J.E. and Plank, R.J. (1991), "Studies of the behaviour of steel beams in fire", *J. Constr. Steel Res.*, **19**, 285-312.
European Committee for Standardization (CEN) (2000), "Design of Steel Structures: Part 1.2: General Rules - Structural Fire Design (EC3 Pt.1.2)", Eurocode 3, British Standards Institution, London.
El-Rimawi, J.A., Burgess, I.W. and Plank, R.J. (1999), "Studies of the ehaviour of steel subframes with semirigid connection in fire", *J. Constr. Steel Res.*, **49**(1), 83-98.
Horne, M.R. and Morris, L.J. (1981), *Plastic Design of Low-rise Frames*, Granada, London.
Huang, Z.F., Tan, K.H. and Ting, S.K. (2006), "Heating rate and boundary restraint effects on fire resistance of steel columns with creep", *Eng. Struct*., **28**(6), 805-817.
Tan, K.H., Toh, W.S. and Huang, Z.F. (2007), "Structural responses of restrained steel columns at elevated temperatures. Part 1: Experiments", *Eng. Struct*., **29**(8), 1641-1652.
Lee, J.H. (2004), *Local Buckling Behaviour and Design of Cold-formed Steel Compression Members at Elevated Temperatures*, Ph.D Thesis, Queensland University of Technology, Australia.
Li, G.Q. and Guo, S.X. (2008), "Experiment on restrained steel beams subjected to heating and cooling", *J. Constr. Steel Res*., **64**(3), 268-274.
Li, G.Q. and Guo, S.X. (2009), "Analysis of restrained heated steel beams during cooling stage", *Steel Compos. Struct*., **9**(3), 191-208.
Liu, T.C.H. (1996), "Finite element modelling of behaviour of steel beams and connections in fire", *J. Constr. Steel Res.*, **35**(3), 181-199.
Liu, T.C.H., Fahad, M.K. and Davis, J.M. (2002), "Experimental investigation of behaviour of axially restrained steel beams in fire", *J. Constr. Steel Res.*, **58**(9), 1211-1230.
Ramli-Sulong, N.H., Elghazouli, A.Y. and Izzuddin, B.A. (2007), "Behaviour and design of beam-to-column connections under fire conditions", *Fire Safety J.*, **42**, 437-451.
Rodrigues, J.P.C., Neves, I.C. and Valente, J.C. (2000), "Experimental research on the critical temperature of compressed steel elements with restrained thermal elongation", *Fire Safety J*., **35**, 77-98.
Santiago, A., Silva, L.S.D., Vaz, G., Real, P.V. and Lopes, A.G. (2008), "Experimental Investigation of the behaviour of a steel sub-frame under a nature fire", *Steel Compos. Struct*., **8**(3), 243-264.
Sarraj, M., Burgess, I.W., Davison, J.B. and Plank, R.J. (2007), "Finite element modelling of steel fin plate connections in fire", *Fire Safety J*., **42**, 408-415.
Tan, K.H. and Huang, Z.F. (2005), "Structural responses of axially restrained steel beams with semi-rigid moment connections in fire", *J. Struct. Eng.-ASCE*, **131**(4), 541-551.
Tan, K.H., Ting, S.K. and Huang, Z.F. (2002), "Visco-elasto-plastic analysis of steel frames in fire", *J. Struct. Eng.-ASCE*, **128**(1), 105-114.
Yin, Y.Z. and Wang, Y.C. (2004), "A numerical study of large deflection behaviour of restrained steel beams at elevated temperatures", *J. Constr. Steel Res.*, **60**, 1029-1047.
Yin, Y.Z. and Wang, Y.C. (2005), "Analysis of catenary action in steel beams using a simplified hand calculation method, Part 1: theory and validation for uniform temperature distribution", *J. Constr. Steel Res.*, **61**, 183-211.
Wald, F., Silva, L.S., Moore, D.B., Lennon, T., Chladná, Santiago A., Beneš and Borges, L. (2006), "Experimental behaviour of a steel structure under nature fire", *Fire Safety J*., **41**, 509-522.
Wang, Y.C., Lennon, T. and Moore, D.B. (1995), "The behaviour of steel frames subject to fire", *J. Constr. Steel Res.*, **35**, 291-322.
Wang, P.J., Li, G.Q. and Guo, S.X. (2008), "Effects of the cooling phase of a fire on steel structures", *Fire Safety J.*, **43**(6), 451-458.
Wong, M.B. (2005), "Modelling of axial restraints for limiting temperature calculation of steel members in fire", *J. Constr. Steel Res.*, **61**, 675-687.

Notations

The following symbols are used in this paper

a : Square section dimension (mm)
E_0^{20} : Elastic modulus at ambient temperature (MPa)
E_0^T : Elastic modulus at temperature T (MPa)
f_y^{20} : Yield strength at ambient temperature (MPa)
f_y^T : Yield strength at temperature T (MPa)
k_l : Linear spring stiffness in horizontal direction (N/mm)
M : Bending moment (N·m)
$M_{p,c}^T$: Beam bending moment at temperature T (Nmm)
M_p^{20} : Plastic bending moment of a section at room temperature 20ºC in absence of axial force (Nmm)
M_p^T : Plastic bending moment of a section at temperature T in absence of axial force (Nmm)
N^T : Beam internal axial force at temperature T (N)
N_y^T : Rigid plastic load of a section at temperature T (N)
N : Internal axial force (N)
N^{20} : Value of N at the beginning of heating (N)
t : Time (min.)
T : Temperature (ºC)
T_{cr} : Beam Critical temperature (ºC)
$T_{\lim}$: Beam limiting temperature (ºC)
T_{ctn} : Beam catenary temperature (ºC)
u^T : Beam end horizontal displacement at temperature T (m)
v^T : Mid-span deflection at temperature T (m)
W_p : Plastic modulus of a section (mm^3)
β_l : Axial restraint ratio
ε_y^T : Yield strain at temperature T
ε_u^T : Ultimate strain at temperature T
ρ_M^{20} : $M_{p,c}^T/M_p^{20}$
ρ_M^T : $M_{p,c}^T/M_p^T$
ρ_N^T : N^T/N_y^T
ξ^T : Plastification index
λ : Slenderness ratio

Right superscript:

20 : 20ºC (room temperature)
T : At elevated temperature T